

**M. Meleddu<sup>1</sup>, F. Foti<sup>2</sup>, L. Martinelli<sup>2</sup>****ODN 0947**<sup>1</sup>Redaelli Tecna Spa, <sup>2</sup>Dep. Of Civil and Environmental Engineering,  
Politecnico di Milano

Redaelli Tecna Spa

Dep. of Civil and Environmental Engineering, Politecnico di Milano, Milano - Italy

## **Temperatures in active heave compensation ropes**

### **Summary**

Utilization of Active Heave Compensation unit (AHC) induces an increase in rope's internal and surface temperatures.

The primary purpose of this experimental research is to analyze the consequences of applying thermal fields on wires. Secondly, to measure the temperature generated, due to rope's back-and-forth movement over a sheave, while having certain inputs for D/d ratio, operation's speed and the applied forces. A Predictive tool to determine the wire rope's temperature variances due to external conditions has been developed by merging the tests' results and the analytical data.

### **1 Introduction**

For many years wire ropes have been used for subsea installations, however, in the recent years there has been a dramatic increase in the requests for wires capable to withstand harsher work conditions. The users need larger and longer ropes which can undergo heavier works and loads. All these has forced the wire rope manufacturers to take part in this quest of better, bigger and more mighty to tackle the ever-larger dynamic loads and the more extreme bending cycles. Active Heave Compensation system (AHC) is one of the factors influencing the most, life expectancy of wire ropes in Abandonment and Recovery applications. AHC is used in order to keep the loads stable respect to the seabed by undermining the water and thus the vessel's movements due to the offshore climate. (1)

The load is kept stable by compensating the wave's state through programmed adjustments to the length of the wire which is involved in the process. These continuous back and forth rope movements respect to the point of equilibrium induce extra stresses on the rope, which are caused by repeated stretching and bending, as well as dynamic loading. These lead to a wear, fatigue and temperature increment on the same portion of the rope, while the payload is static with respect to the seabed. The fatigue damages characteristics of steel wire rope throughout its service life, which has been topic of an in-depth study by Schrems K (2, 8). Many studies have been carried out during the years on the smaller ropes while there is a lack of information and studies on larger diameters, moreover, the effect of temperature on the mechanical behaviour of the ropes has not been tackled in-depth yet (9).

This research through laboratory tests has investigated the heat which is generated due to ropes bending over a sheave and how the external conditions could affect this phenomenon.

### **1.1 Thermal effect on high hardened steel wire**

The process leading the variation of mechanical properties on high carbon drawn steel wire has been largely investigated for years (3, 4, 10). Nevertheless, we concentrate our investigation on specific window of interest in terms of temperature and related mechanism leading the heating generation.

In detail, this research is carried out in order to investigate the amount of heating generated on a rope during an intense use of AHC in a range of temperature from 25°C to 150°C. This range of temperature is chosen in accordance to the mean dropping point temperature of various lubricants required for ropes in offshore applications.

Under thermal cycling exposition, the high-hardened drawn wires undergo changes in their mechanical properties. These characteristics are the Breaking Strength ( $R_m$ ), Yield Strength ( $R_{p0.2}$ ) and the Elongation at break ( $Ez$ ), defined as:

$Ez = 100 (L-L_0)/L_0$  where  $L_0$  is the initial length of the wire and  $L$  is the length of the wire at break.

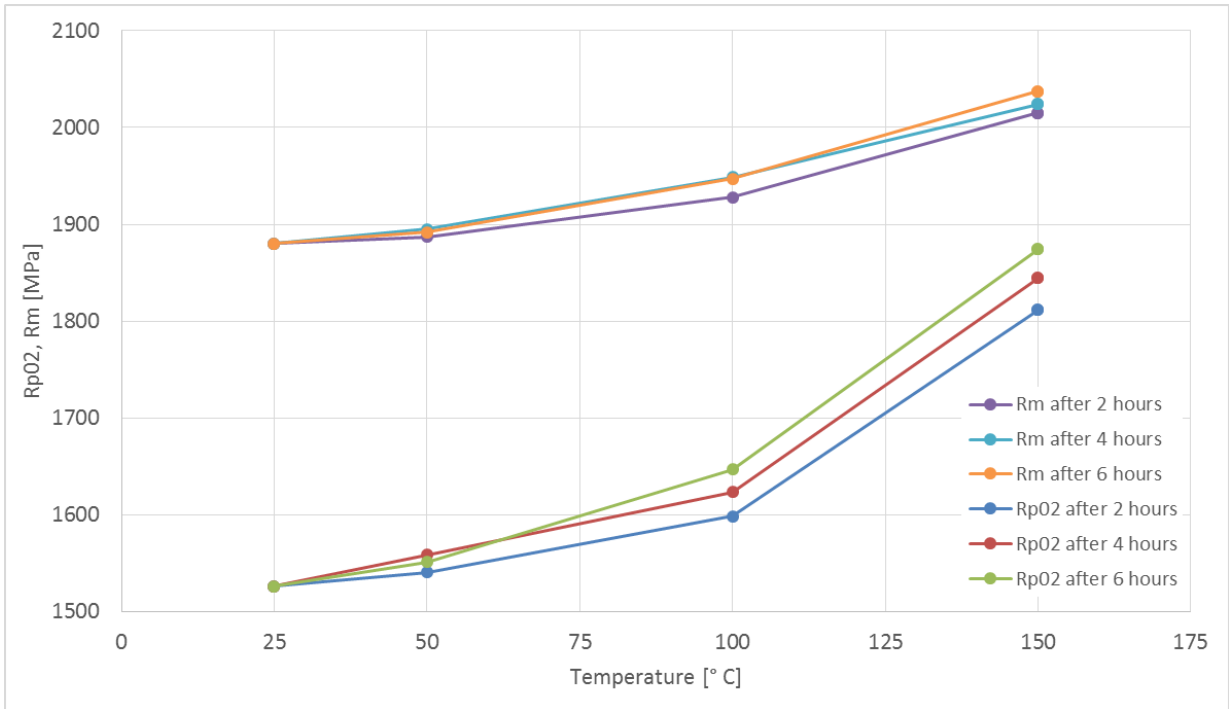
The investigation of these changes highlights a faster deterioration of material's ductility when the wires are exposed to a thermal field within the range of 50°C to 150°C (according to data gathered from the field).

Our analysis show how a thermal influence within the mentioned range of temperature (in accordance to the data coming from the field) induces a fast deterioration of ductility.

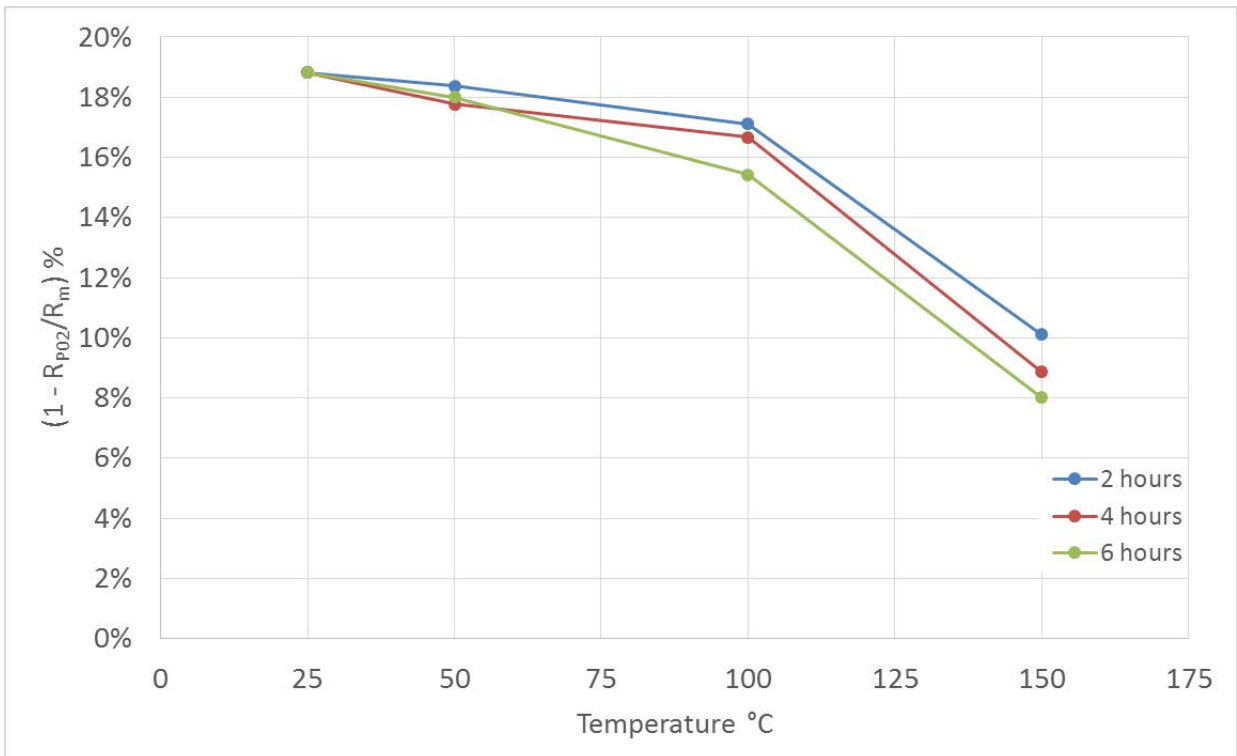
Hundreds of high carbon steel wires (diameter 3,03, length 300 mm) have been submitted to different thermal conditions (at 25, 50, 100, and 150 °C) for various time frames of 2, 4 and 6 hours. After the thermal treatments, all the groups have been tested at room temperature and the relative results have been plotted for a comparison.

Results are summarised as per the followings.

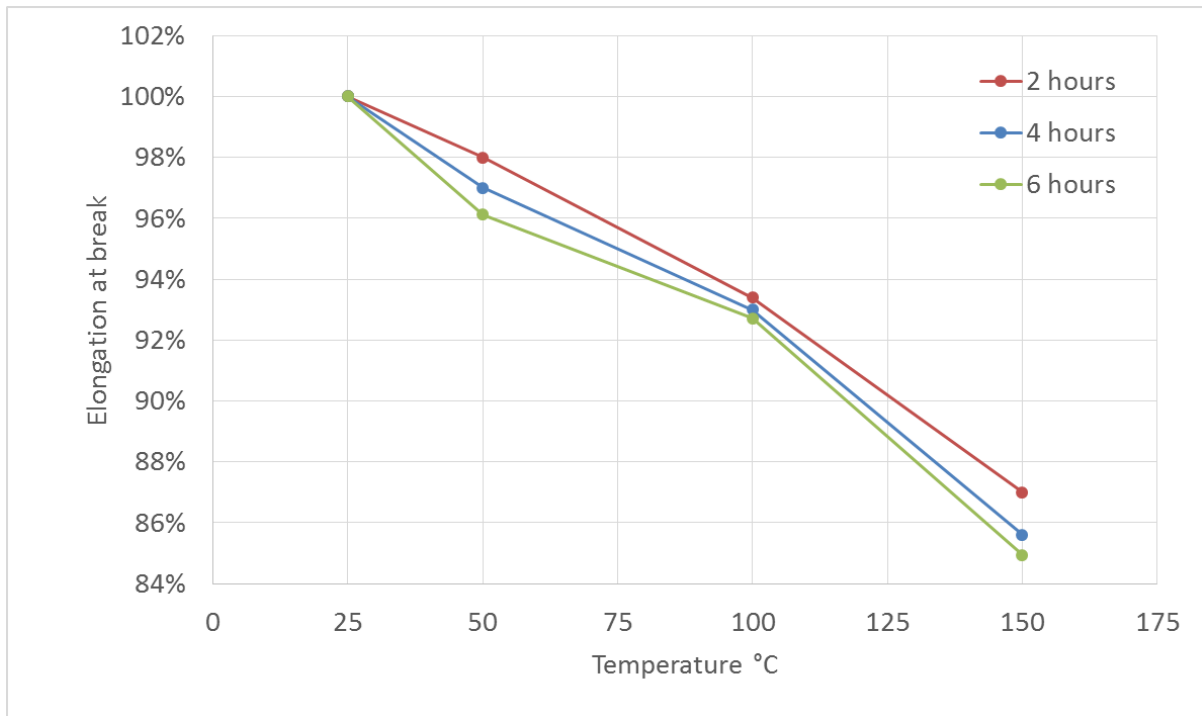
Graph 1 represents the  $R_{p0.2}$  and  $R_m$  values obtained at different temperatures after 2, 4 and 6 hours of exposition (4), graph 2 represents the  $R_{p0.2}/R_m$  ratio; graph 3 represents the elongation at break over the temperature with respect to the reference value at 25°C. All the plotted characteristics, within the examined range of temperatures, show a decrease of ductility.



**Graph 1:** Rp02 and Rm over the Temperature



**Graph 2:** (1- Rp02 / Rm) over the Temperature



**Graph 3:** Elongation at break variation over the Temperature

### 1.2 Heating generation. Rope and sheave's interaction

The investigation studies the correlation between AHC operational conditions (speed, frequency,  $D/d$  ratio, ambient temperature) and the consequent achieved temperatures. For this scope, several bending tests have been run

Unfortunately, some limitations induced by the available testing machine have to be taken into account. The tests have been run at IFT laboratory where the biggest bending-test machine has the full scale applicable load of 500 kN and highest rope speed 0.4 m/s (which for our configuration corresponds to a time cycles of 32s). The most representative and suitable rope for our purpose is a rotational resistant rope,  $\Phi$  52 mm, class 39(W) x K7 with a nominal MBL of 2500 kN

Furthermore, the limitation on the max applicable speed permitted to apply only time cycles of 32 and 64 seconds per cycle, which are quite far from the real scenarios.

The inner temperature is monitored through a thermocouple placed into the king strand's core, and the outer one has been monitored through a thermal camera. The two devices have been calibrated on the same temperature readings.

### 1.2.1 Tests Setup

Temperature data collected by some end users turns within a range of 100 – 150 °C (and sometime even more), mean wave amplitude  $\pm 3 / \pm 4$  meters compensated in 2.3-2.5 m/s.

Due to testing machine limitations, the range of applicable conditions are limited in Rope diameter, Pulling force and Frequency.

The test setups consist of:

- Non rotating rope class 39(w) x K7
- Diameter  $\Phi$  52 mm
- Rope breaking load 2500 kN
- Bending length 2000, 2300 mm
- Rope speed: 0.1 m/s and 0.4 m/s, corresponding to 64 s and 32 s of time cycle
- Sheave for test 1  $\Phi$  1040 mm, D/d ratio: 20
- Applied loads 250 kN, 357 kN and 500 kN
- Sheave for test 2  $\Phi$  780 mm: D/d ratio: 15
- Applied loads 250 kN, 357 kN and 480 kN

All the mentioned input (Loads, speeds, D/d) are combined, and the reported in table 1, with the scope of obtaining a matrix of possible cases of interest

Test 1 - D/d = 20			
Load [kN]	speed [m/s]	time cycle[s]	safety factor
250	0.1	64	10
	0.4	32	10
357	0.1	64	7
	0.4	32	7
500	0.1	64	5
	0.4	32	5

**Table 1:** Matrix of input for Test 1

Since the highest limit of impossible load on the bending test machine could not exceed 500 kN and the consequent lowest safety factor is 5 (which corresponds to the double of what normally is used in A&R systems), we decided to induce a higher rope stress by reducing the D/d ratio from 20 to 15.

Test 2 - D/d = 15			
Load [kN]	speed [m/s]	time cycle[s]	safety factor
250	0.1	64	10
	0.4	32	10
357	0.1	32	7
	0.4	32	7
480	0.1	32	5
	0.4	32	5

**Table 2:** Matrix of input for Test 2

During the last 3 tests, the elongation of the driving rope induced a new testing machine adjustment and consequently the max applicable load reduces to 480 kN

In the following pictures the testing machine set up, and an example of thermal map obtained during the D/d15 test at 0,4 m/s under 480 kN pulling force are presented.

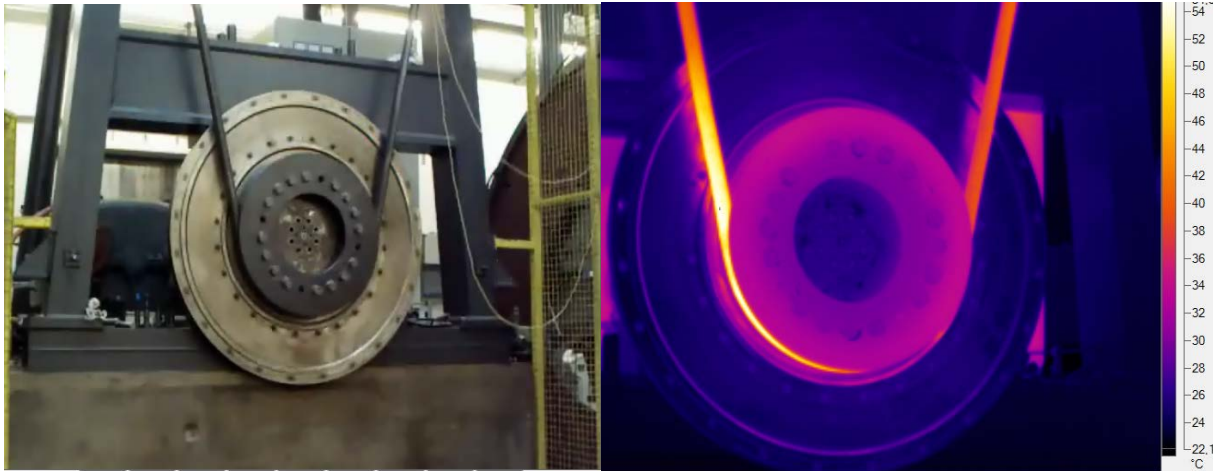
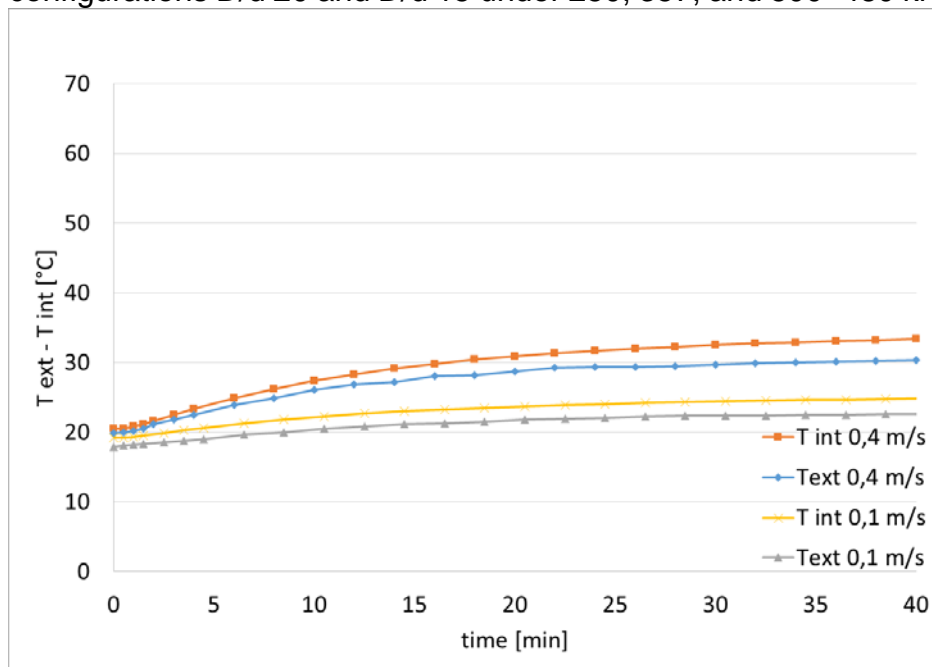


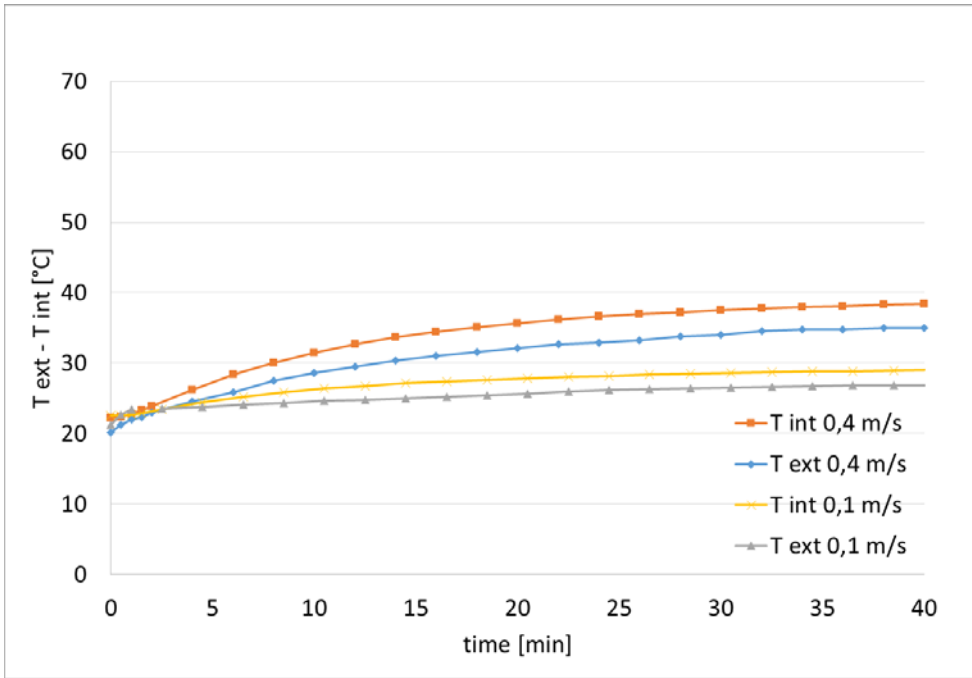
Figure1: Test setup - thermal acquisition throughout a thermal camera and thermocouples

### 1.3 Results

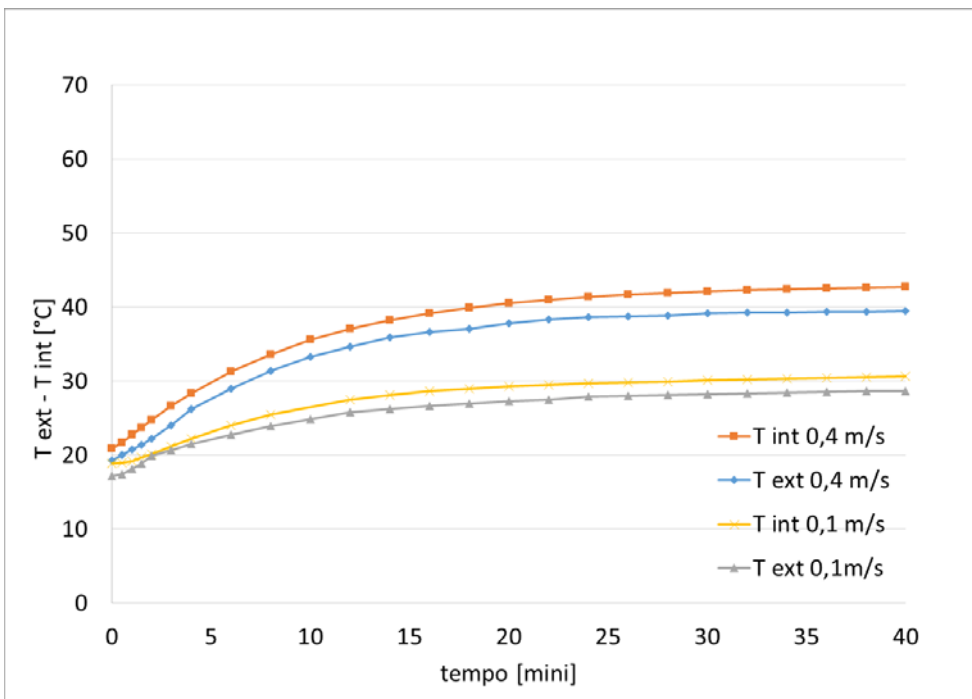
The following graphs represent the recorded inner and outer temperatures for both test configurations D/d 20 and D/d 15 under 250, 357, and 500- 480 kN, at 0.1 and 0.4 m/s.



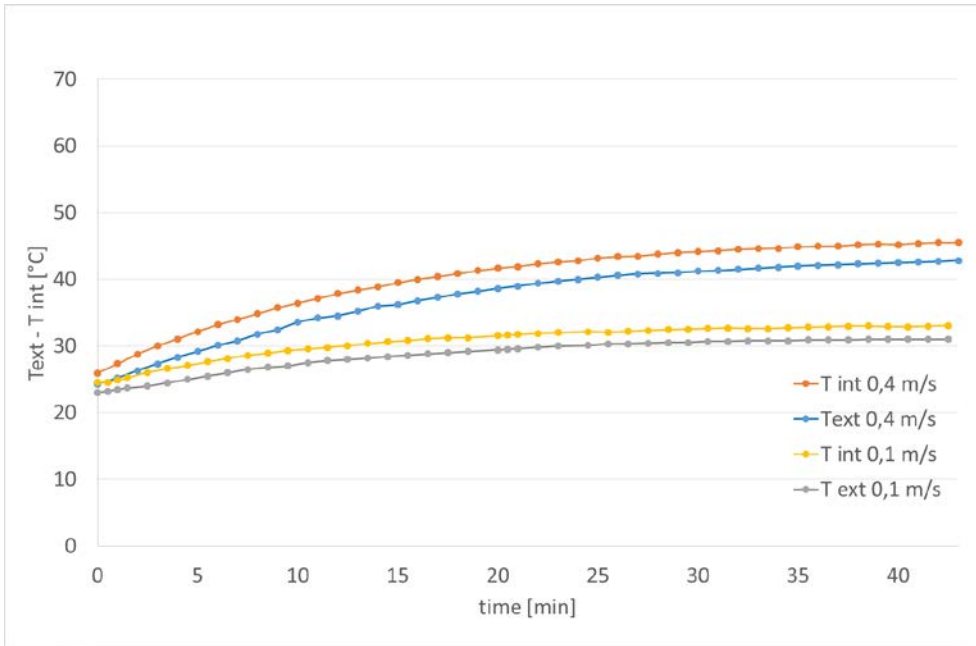
Graph 3: inner- outer Temperature at 0.1 m/s and 0.4 m/s at D/d 20 and 250 kN



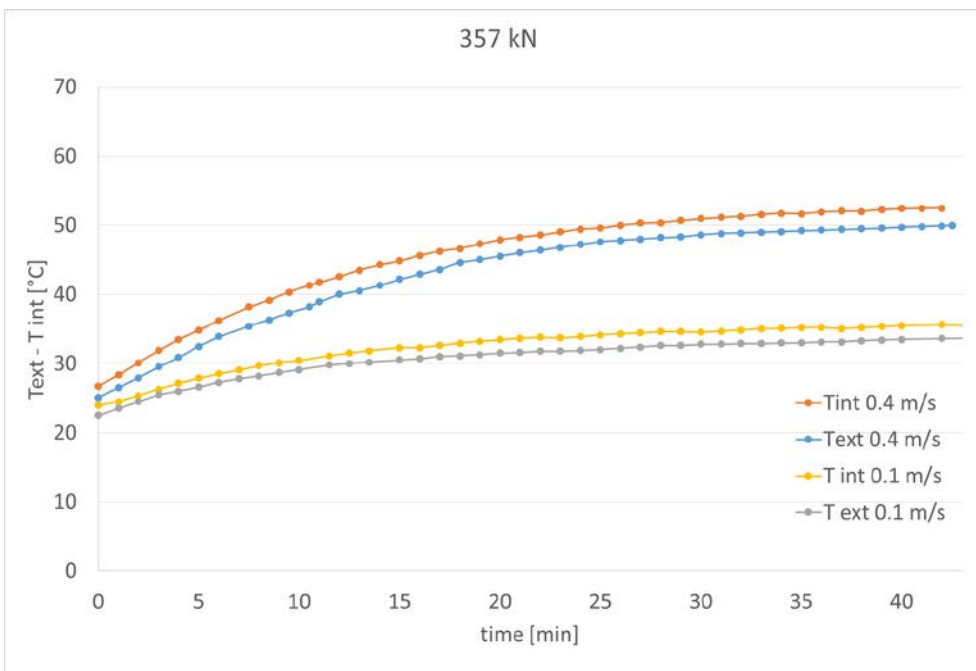
**Graph 4:** inner- outer Temperature at 0.1 m/s and 0.4 m/s at D/d 20 and 357 kN



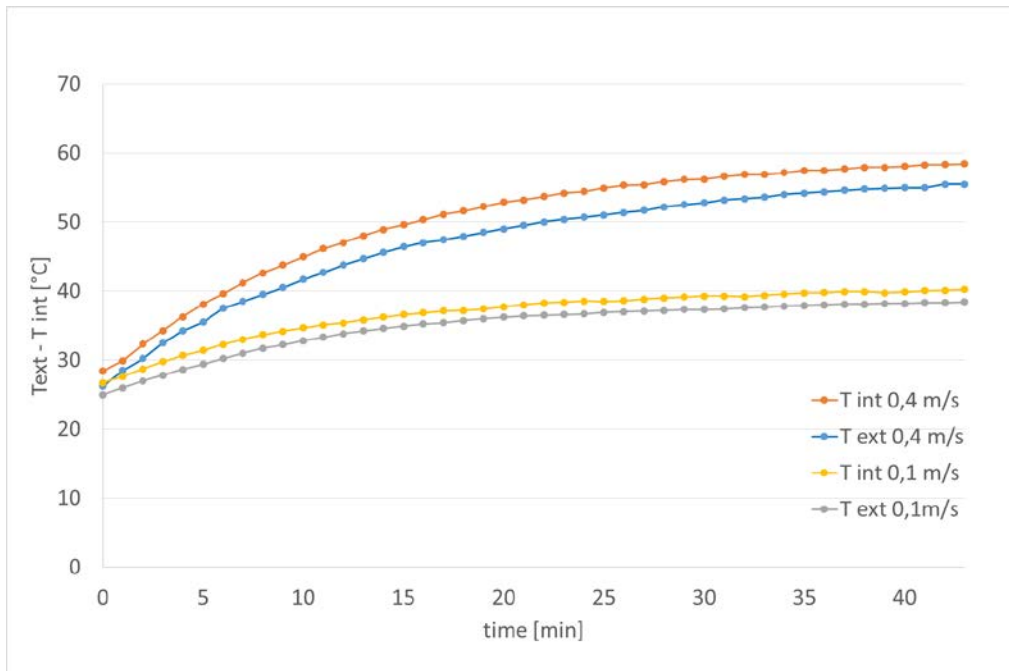
**Graph 5:** inner- outer Temperature at 0.1 m/s and 0.4 m/s at D/d 20 and 500 kN



**Graph 6:** inner- outer Temperature at 0.1 m/s and 0.4 m/s at D/d 15 and 250 kN

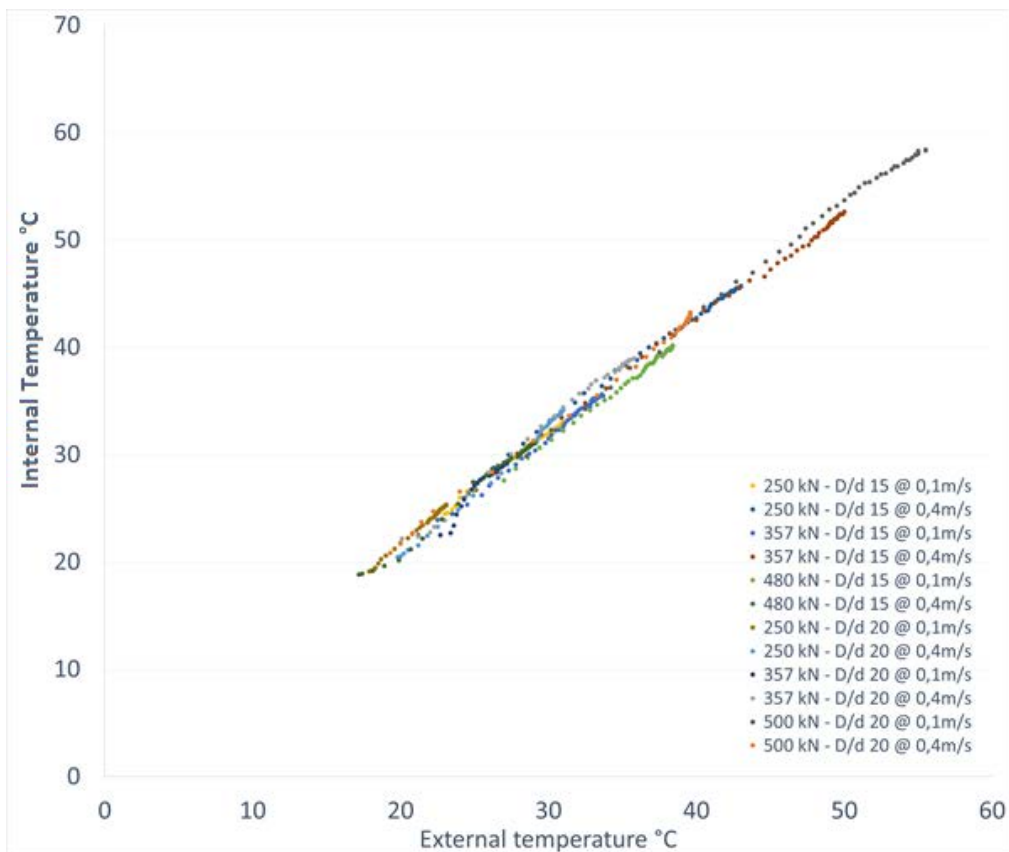


**Graph 7:** inner- outer Temperature at 0.1 m/s and 0.4 m/s at D/d 15 and 357kN



**Graph 8:** inner- outer Temperature at 0.1 m/s and 0.4 m/s at D/d 15 and 480 kN

The direct conclusion is the increase of the max final temperatures by increasing the applied load and speed, while they would be increased even more by reducing the D/d ratio. The following graph (9) represents the relationship between the external and internal temperatures recorded during all the tests both at 0,1m/s and 0,4 m/s and both for D/d 15 and 20 configuration



**Graph 9:** external internal rope temperature for the all applied configuration

The results indicate that the applied speeds and loads influence the max temperature and does not affect the slope of the correlation. The same linearity is maintained on both tests with  $D/d=20$  and  $D/d=15$  configurations.

The recorded inner and outer temperatures during the tests led to determination of the wire rope’s internal and external thermal variation ( $\Delta T$ ) with respect to the environment temperature. During all tests the ambient temperature was stable approximately within the range of 22-23 °C.

In the following tables both variations between internal/external and ambient temperature are reported;

D/d 20 @ 0.1 m/s		
Load (kN)	$\Delta T_{ext}$ measured °C	$\Delta T_{int}$ measured °C
250	5.6	7.8
357	9.8	11.9
500	11.7	13.6

**Table (3):** Temperature variations with respect to the ambient temperature for  $D/d$  20 and 0,1 m/s

D/d 15 @ 0.1 m/s		
Load (kN)	$\Delta T_{ext}$ measured °C	$\Delta T_{int}$ measured °C
250	8.0	10.1
357	10.7	12.7
480	15.4	17.3

**Table (4):** Temperature variations with respect to the ambient temperature for  $D/d$  15 and 0.1 m/s

The results obtained in all tests’ configurations have been used to calibrate the predictive thermal model, which as a primary scope simulates the same experimental tests and secondly is intended to extend the simulation to other configurations.

## 2 Numerical modelling of the tests

### 2.1 Geometry of the rope

The approach adopted in this paper to describe the geometry of wire ropes is to view them as composite structures obtained through assemblies of helical components in hierarchical levels [1]: the strands are helically twisted and grouped in concentric layers to form the rope and the same process forms the strand from the wires.

The internal structure of the rope is completely defined by the centreline and the orientation of the transversal section of every element at each level. As an example, with reference to the wire rope in Figure 2, the following levels can be identified: wires, strands and the rope itself, and on each element a local reference system can be defined by the Serret-Frenet unit vectors. The strand centreline is described by a cylindrical helix in the frame of reference of the rope while a wire centreline is described by a cylindrical helix in the frame of the strand (and by a double, or nested, helix in the frame of the rope [2, 3]).

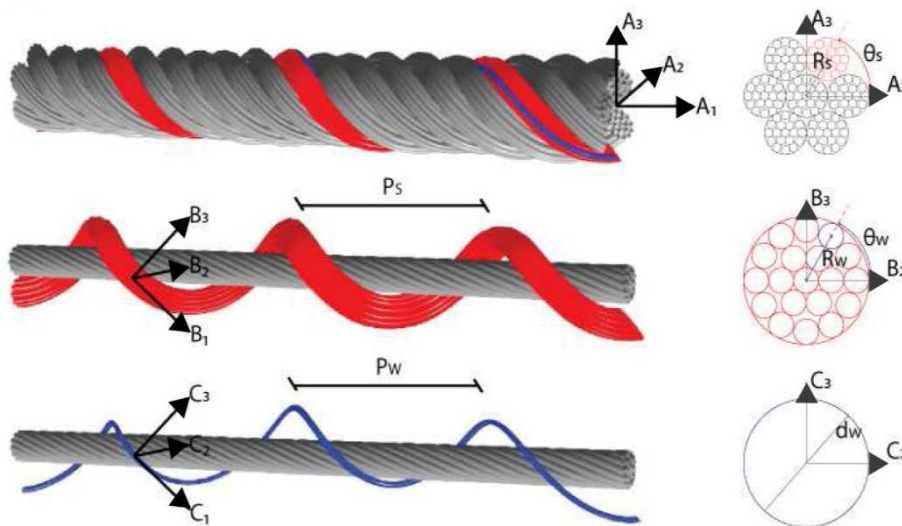
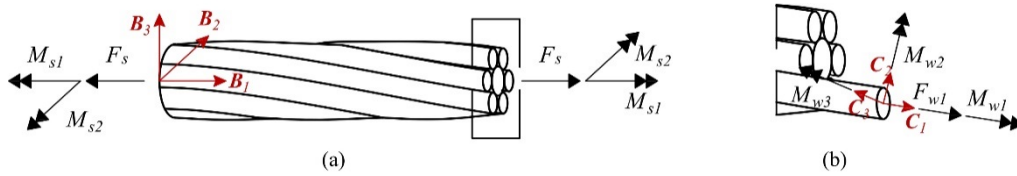


Figure 2: Internal geometry of the wire rope.

The position and orientation of a component cross section in the frame of the component at the higher hierarchical level is hence completely defined as a function of two construction parameters (the helix radius  $R$  and the pitch  $P$ ) and of the swept angle  $\theta$  (e.g.  $R_w$ ,  $P_w$  and  $\theta_w$  for a wire in a strand, or  $R_s$ ,  $P_s$  and  $\theta_s$  for a strand in a rope). Further details on the mathematical model adopted in this work to describe the geometry of the wires can be found in [4] and [5].

### 2.2 Mechanical model of the strand

The response of the strand to mechanical loads is characterized as elastic and will be evaluated by neglecting friction between the wires and modelling each wire as a curved thin rod, reacting to a combination of axial force, bending and torsional moments (see Figure 3). The material properties of each wire are fully defined, under the assumption of linear elastic behaviour, by specifying the Young modulus  $E$  and the Poisson coefficient  $\nu$ .



**Figure3:** (a) Straight strand subjected to a combination of axial-torsional and bending loads, (b) generalized stresses on the wire cross section.

The stress resultant on the strand cross section is described by introducing the axial force  $F_s$ , the torsional moment  $M_{s1}$  and the bending moment  $M_{s2}$ . The generalized strains, work-conjugated to the cross sectional stress resultants of the strand are the axial strain  $\varepsilon_s$ , the torsional curvature  $\chi_{s1}$ , and the bending curvature  $\chi_{s2}$ . Without loss of generality, a planar bending problem is herein considered, referring e.g. to [5] for a full discussion of the kinematical assumptions at the base of this formulation and of the case of biaxial bending. By neglecting variations of the internal geometry of the strand, the following linear cross sectional constitutive equations can be introduced:

$$\begin{cases} F_s = EA_s \varepsilon_s + C_s \chi_{s1} \\ M_{s1} = C_s \varepsilon_s + GJ_s \chi_{s1} \\ M_{s2} = EI_s \chi_{s2} \end{cases} \quad (1)$$

In the equations above  $EA_s$ ,  $GJ_s$  and  $EI_s$  denote, respectively, the direct axial, torsional and bending stiffness coefficients, while  $C_s$  is the axial-torsional coupling stiffness term. The stiffness coefficients of the strand are evaluated in this work by means of the equations derived in [5], here omitted for the sake of conciseness.

### 2.3 Mechanical model of the rope

The “two-stage” approximate approach outlined by Cardou and Jolicoeur [6] is retained also in this work to model the cross-sectional behaviour of a rope subjected to the combined action of the tensile load  $F_r$  and of the imposed bending curvature  $\chi_r$ . Accordingly, the solution of the bending problem is superimposed to the initial state of stress and strain due to the tensile load and the following constitutive equations are introduced under the assumption of restrained torsional rotations:

$$\begin{cases} F_r = EA_r \varepsilon_r \\ M_r = EI_{\min} \chi_r + M_r^{add}(\varepsilon_r, \chi_r) \end{cases} \quad (2)$$

where:  $\varepsilon_r$  and  $M_r$  are the axial strain and the resultant bending moment of the rope, respectively.

The axial behaviour is assumed to be independent on the bending curvature and the direct axial stiffness of the rope can be estimated as follows:

$$EA_r = \sum_{j=0}^m n_j \cos^3(\alpha_{s,j}) EA_{s,j} \quad (3)$$

where:  $m$  is the number of layers of the rope;  $n_j$  is the number of strands belonging to the  $j$ -th layer (the index  $j = 0$  refers to the core of the rope), and  $\alpha_{s,j} = \tan^{-1}(2\pi R_{s,j}/P_{s,j})$  is the lay angle of the strands in the  $j$ -th layer.

Two different contributions to the rope bending moment  $M_r$  can be recognized in the Eq. (2). The first one is linear and independent of the axial strain of the strand. This term is defined taking into account only the individual bending of the strands and can be also regarded as the theoretical response of the rope under the ideal condition of ‘full-slip’ described by Hobbs and Raof (see e.g. [7, 8]), with no friction between the strands (or, in other terms, under the assumption of *perfectly lubricated strands*). Accordingly, the subscript ‘*min*’ is adopted in this work to further highlight that this contribution corresponds to the minimum theoretical value for the cross sectional bending stiffness of the rope. By following the approach described in [5], the stiffness coefficient  $EI_{min}$  can be defined as:

$$EI_{min} = \sum_{j=0}^m \frac{n_j}{2} \cos(\alpha_{s,j}) \left( \sin(\alpha_{s,j}) GJ_{s,j} + (1 + \cos^2(\alpha_{s,j})) EI_{s,j} \right) \quad (4)$$

The second term in Eq. (2),  $M_r^{add}$ , is non-linear and accounts for the contribution to the total bending moment of the cross section due to the axial force,  $F_s$ , acting in the individual strands. From simple equilibrium considerations, the following expression can be obtained:

$$M_r^{add} = \sum_{j=0}^m \sum_{i=1}^{n_j} R_{s,j} \cos(\alpha_{s,j}) F_{s,i}(\theta_{s,i}) \sin(\theta_{s,i}) \quad (5)$$

The axial force acting in the generic strand can be further decomposed into a first contribution,  $F_{s,a}$ , due to the axial load  $F_r$ , and a second one,  $F_{s,b}$ , due to the bending of the strand, i.e.:  $F_s = F_{s,a} + F_{s,b}$ .

Due to the cylindrical symmetry of the axial-torsional problem with respect to the centreline of the rope, the term  $F_{s,a}$  is a constant along the length of the strand (and over all the strands of the same layer).

As long as the friction forces on the external surface are large enough to prevent relative displacements between the strands, i.e. in a strand stick-state [9], the force  $F_{s,b}$  can be evaluated as:

$$F_{s,b}(\theta_s) = \cos^2(\alpha_s) R_s EA_s \sin(\theta_s) \chi_r \quad (6)$$

The term  $F_{s,b}$  generates a gradient of axial force along the strand, as can be easily derived from (6). This gives the strands a tendency to slip with respect to the neighbouring ones. This gradient of axial force is resisted by the tangential friction forces acting on the lateral surface of the strand. Whenever the effect of the axial force gradient is greater than the resultant of the tangential friction forces, a strand can undergo a relative displacement with respect to the neighbouring ones. A numerical strategy to evaluate the strand axial force  $F_{s,b}$ , accounting for the possible transition between a sticking and a slipping regime has been developed by the authors in [4, 5, 10] and is adopted also in this work. The numerical procedure is based on a classic Return-Map algorithm, based on a “sticking regime prediction” and a “sliding regime correction”. The Return-Map algorithm delivers the value of the gradient of the strand axial force at a discrete set of control points along the pitch of the strand. Then, the strand axial force is obtained through numerical integration along the strand length.

This friction-based mechanism for the transmission of shearing stresses between the strands makes the bending behaviour of the rope non-linear. Figure 4 shows a typical cross sectional moment-curvature hysteresis loop predicted by the proposed model. A cyclic curvature with limits  $\pm\chi_{max}$  is applied to the cross section. The initial branch is characterized by the initial stiffness  $EI_{max}$ , corresponding to the ‘full-stick’ case (no relative displacement between the strands, see also [7, 8]). The tangent stiffness, then, gradually decreases as a consequence of the evolution of the inter-strand sliding phenomena. Note that  $\chi_{max}$  is assumed as sufficiently large to achieve the limit value  $EI_{min}$ , which can be attained only if all strands of the cross section are in the slipping state.

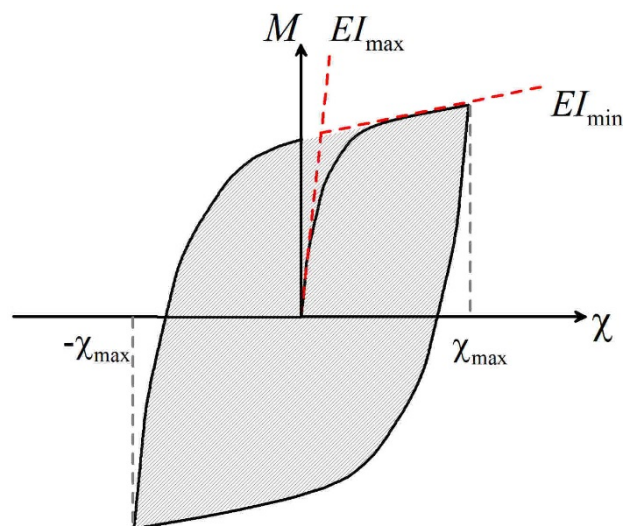


**Figure 4:** Cross sectional bending response of the rope.

Whenever a rope is bent over a sheave having diameter  $D$ , three regions can be easily defined according to the value of the curvature of its centreline. In the first one, which

is far from the sheave, the rope centreline is straight and its curvature is strictly equal to zero. In the second one, which is on the contact region between the rope and the sheave, the curvature of the rope centreline is constant and can be approximately evaluated as:  $\chi_{max} = 2/D$ . The third region, which is characterized by the transition between the zero curvature and the maximum curvature  $\chi_{max}$  imposed by the sheave, is neglected in this work. A generic cross-section of the strand passing over the sheave will be considered as bent from zero to the final curvature value  $\chi_{max}$ . The energy dissipated during the bending of the cross section (dissipated energy per unit length of the strand) can be evaluated as the area  $A_c$  enclosed in the hysteresis loop:

$$A_c = \oint M_r(\chi_r) d\chi_r \quad (7)$$

## 2.4 Thermal model

Whenever a strand or a wire rope is cyclically bent over a sheave, a portion of the total mechanical power provided as input to the system is dissipated through frictional phenomena and transformed in heat. The generated heat is then transmitted through the strand and exchanged with the environment.

Two main dissipation sources can be identified: (1) the friction between the strand (or rope) and the sheave; and (2) the friction between the components of the strand (or rope). The first source of dissipation, could be relevant in some practical operating conditions but is usually negligible in laboratory testing conditions like the ones considered in this work. The second one, instead, is always present and cannot be ignored, being inherently related to the alternate bending and straightening of the rope cross sections. The heat generation source  $g$  can then be estimated simply from the energy  $A_c$  (Nm/m) in Equation 7, dissipated per unit of length over a full bending cycle (from zero to the curvature  $\chi_{max}$  imposed by the sheave, and back to zero again).

In order to estimate the steady-state temperature distribution of the rope, the heat source  $g$  has been considered as constant along the contact arc between the rope and the sheave. The maximum steady-state temperature of the rope bent over sheave has been, accordingly, estimated through the following heat balance equation:

$$q_c + q_r = g + q_s \quad (8)$$

where:  $q_c$  is the conducted heat loss,  $q_r$  is the radiated heat loss,  $q_s$  is the solar heat gain.

## 2.5 Simulation of experimental tests

The predictions of the numerical model are here compared to the results of the experimental tests. The wire rope is bent over sheaves with diameters  $D = 780$  mm and  $D = 1040$  mm and a velocity of 0.1 m/s. The rope is subjected to three different values of axial load: 250 kN, 357 kN and 500 kN, which correspond to the 10%, 14% and 20% of the rope MBR, respectively.

Figure 6 compares the increment of the external temperature coming from the numerical model versus the values measured inside the rope and on its surface, already reported in Table 3, as a function of the axial load.

Numerical results are shown for three different values of the interstrand friction coefficient  $\mu$ , that can be considered to fall in the range of values representative of well lubricated contact patches.

It can be observed that the proposed model, for given speed, load,  $D/d$  ratio and room temperature, is capable to estimate reasonably well the average rope temperature. This opens the way for correlating the operational boundary conditions to the rope temperature also in different and more complex scenarios.

Figure 5 also allows to appreciate that a 20% variation in the value of the friction coefficient leads to variation of the same order of magnitude of the predicted rope temperature. This observation points out the need for a proper choice of the value of the friction coefficient used as input to the proposed model. Literature experimental data (see e.g. [11]) can be used to guide the choice of the interstrand friction coefficient. However, it's worth noting that the friction coefficient is a quantity difficult to measure, affected by many uncertainties and strongly varying with the time (rope ageing) and lubrication conditions [12]. The combined use of the experimental and analytical approach presented in this paper, however, allows to easily estimate the model parameter  $\mu$  from the measurement of rope temperature. The latter point is of special interest for future research aimed at investigating the internal dissipation properties of strands and wire ropes.

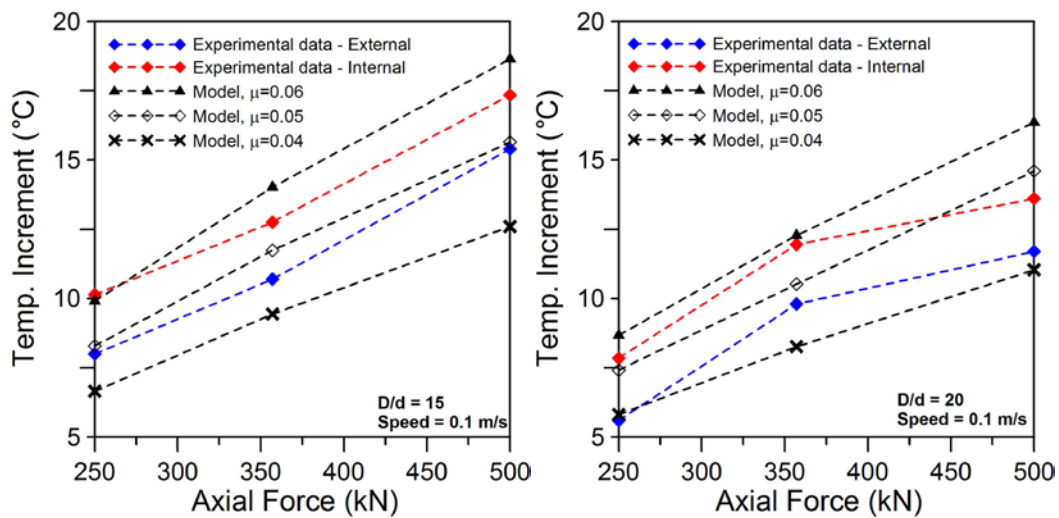


Figure 5: Experimental versus numerical temperature increments.

### 3 Conclusion

The obtained experimental results permit the evaluation of internal and external temperature variations while a non-rotating rope runs over a sheave under different loading and speed conditions.

Even though the calibration of the predictive tool is obtained through a restricted number of cases, the authors are confident that extension to other cases is possible with quite good certitude. Nevertheless, it is certain that more data should be captured in real operational conditions in order to enhance the level of confidence in the predictive outcomes.

## References

### Experimental part

- (1) Kirstein, H, *Active Heave Compensation Systems on Board of Vessels and Offshore Rigs*, Marine Technology, 17, 59-61, 1986
- (2) Schrems K.K. *Wear-related fatigue in a wire rope fatigue*. Journal of Testing and Evaluation, 22, 490–499, 1994.
- (3) Strain ageing and delayed failure in high-strength steels Thompson Ramo Wooldridge Inc., Cleveland, Ohio;E. A. Steigerwald and G. L. Hanna, authors.J, 1961-1962
- (4) Strain ageing in ultra-high strength drawn pearlitic steels, Nicholas Tau J Widdrington Davies, 1987
- (5) Chaplin C.R. Failure mechanism in wire ropes, Engineering Failure Analysis, 2, 45–57, 1995
- (6) Jeong In Suh, Sung Pil Chang. Experimental study on fatigue behaviour of wire ropes. International Journal of Fatigue, 22, 339-347, 2000
- (7) Kim S. H., Bae R. H., Kwon J. D.. Bending fatigue characteristics of wire rope. Journal of Mechanical Science and Technology,7, 2017–2110, 2012
- (8) Zhang D., Chen K., Jia X., Wang D., Wang S., Luo Y., Ge S., Bending fatigue behaviour of bearing ropes working around pulleys of different materials, Engineering Failure Analysis 33, 37–47, 2013
- (9) Chen K., Jia X., Wang D., Wang S., Luo Y., Ge S., Bending fatigue behaviour of bearing ropes working around pulleys of different materials, Engineering Failure Analysis 33, 37–47, 2013

- (10) Lamontagne A., Massardier V., Sauvage X., Kleber X., Man D., Zhang D., Evolution of carbon distribution and mechanical properties during the static strain ageing of heavily drawn pearlitic steel wires *Materials Science & Engineering A*, A 667, 115-124, 2016

### Numerical Part

- [1] Leech, C.M. *The modelling of friction in polymer fibre ropes*, *International Journal of Mechanical Sciences* 44: 621–643, 2002.
- [2] Usabiaga, H., Pagalday, J.M. *Analytical procedure for modelling recursively and wire by wire stranded ropes subjected to traction and torsion loads*, *International Journal of Solids and Structures* 45: 5503-5520, 2008.
- [3] Feyrer, K. *Wire ropes: Tension, Endurance, Reliability*, Berlin: Springer-Verlag, 2007.
- [4] Foti, F. *A corotational beam element and a refined mechanical model for the nonlinear dynamic analysis of cables*, Doctoral Dissertation, Politecnico di Milano, 2013.
- [5] Foti, F., Martinelli, L. *Mechanical modeling of metallic strands subjected to tension, torsion and bending*, *International Journal of Solids and Structures* 91: 1-17, 2016, 2016.
- [6] Cardou, A., Jolicoeur, C. *Mechanical models of helical strands*, *Applied Mechanics Reviews ASME* 50: 1-14, 1997.
- [7] Raoof, M., Hobbs, R.E. *Analysis of multilayer structural strands*, *Journal of Engineering Mechanics ASCE* 114: 1166-1182, 1988.
- [8] Hobbs, R.E., M., Raoof *Behaviour of cables under dynamic of repeated loading*, *Journal of Constructional Steel Research* 39: 31-50, 1996.
- [9] Papailiou, K.O. *On the bending stiffness of transmission line conductors*, *IEEE Transaction on Power Delivery* 12: 1576-1588, 1997.
- [10] Foti, F., Martinelli, L., Perotti, F. *A new approach to the definition of self-damping for stranded cables*, *Meccanica* 51: 2827-2845, 2016.
- [11] Urchegui, M.A., Hartelt, M., Klaffke, D., Gómez, X. *Laboratory fretting tests with thin wire specimens*, *Tribotest* 13: 67-81, 2007.
- [12] Raoof, M., Huang, Y.P. *Upper-bound prediction of cable damping under cyclic bending*, *Journal of Engineering Mechanics ASCE* 117: 2729-2747, 1991.